geoconvention
Calgary • Canada • May 7-11 2018

Waveform Calibration of Time-Lapse Seismic Data

Yichuan Wang and Igor B. Morozov
University of Saskatchewan
yichuan.wang@usask.ca, igor.morozov@usask.ca

Summary

In time-lapse seismic imaging, calibration for time-lapse reflection waveforms is a key step of measuring the reflectivity and impedance changes within the target zone. Here, we describe an approach to such calibration using a combination of conventional time shifting and amplitude and spectral corrections with instantaneous waveform attributes. Instantaneous-attribute based calibration helps to achieve more accurate waveform matching as well as accurate estimates of time-lapse reflectivity and impedance differences within the target zone. The approach is illustrated on time-lapse 3-C 3-D datasets from the Weyburn CO_2 sequestration project in southern Saskatchewan, Canada.

Introduction

Time-lapse reflection seismic methods (Greaves and Fulp, 1987; Lumley, 1995; Johnston et al., 1998) are widely used in reservoir monitoring and geological CO_2 sequestration studies. These methods are based on equalizing (calibrating) the monitor and baseline seismic records and measuring small differences of reflectivities and derived quantities (amplitudes, impedances) occurring over the time-lapse period. Accurate waveform calibration methods are thus critical for such measurements.

Two different groups of calibration procedures are included in our approach: 1) time-variant window-based calibration and 2) instantaneous attribute-based calibration. The window-based calibration is similar to the cross-equalization method (Ross et al., 1996) and contains three components: time shifting, amplitude correction and spectral correction of monitor records. The second procedure 2) is new and uses corrections of the instantaneous amplitudes and phases of the monitor records. These two groups of operations are performed twice: first in order to remove the differences caused by different acquisition and seismic processing conditions, and second, in order to evaluate the time-lapse reflectivity and impedance differences within the target zone.

In the following sections, these two calibrations are described separately and reflectivity difference of Weyburn Field is calculated after these calibrations.

Method

Time-variant window-based calibration

The first calibration approach is based on time-variant filtering implemented by using a series of overlapping Hanning time windows constructed within the baseline and monitor traces (Wang and Morozov, 2017). Denoting the baseline and monitor records tapered within one window by $u_{\mathrm{bas}}(t)$ and $u_{\mathrm{mon}}(t)$, the calibrated monitor signal $u_{\mathrm{cmon}}(t)$ is obtained by applying linear filters f_{tim}, f_{amp} and f_{spec} to $u_{\mathrm{mon}}(t)$. These filters perform time shifting, amplitude correction and spectral correction, respectively:

$$u_{\mathrm{cmon}} = u_{\mathrm{mon}} * f_{\mathrm{tim}} * f_{\mathrm{amp}} * f_{\mathrm{spec}}, \qquad (1)$$

where '*' denotes the convolution operation. For each of these three filters, the approprate parameters are measured at the center of the corresponding window and linearly interpolated between adjacent windows.

The filters in eq. (1) are implemented as follows. First, filter f_{tim} is applied as a shift by time increment Δt. Within each time window, the value of Δt required for calibration is obtained by maximizing the cross-correlation of the monitor signal with the corresponding windowed record of the baseline survey. After time shifting, the spectral-shaping filter f_{spec} is applied by scaling the amplitude spectrum $A_{\text{mon}}(f)$ in the frequency domain:

$$A_{\text{cmon}}(f) = A_{\text{mon}}(f)\mathrm{e}^{-\pi(f-f_0)t^*}, \qquad (2)$$

where f_0 is the dominant frequency, and parameter t^* is estimated so that $A_{\text{cmon}}(f)$ approximates the spectrum of baseline record ($A_{\text{bas}}(f)$) by linear regression. The amplitude-correction filter f_{amp} is performed by simple scaling:

$$u_{\text{cmon}}(t) = s u_{\text{mon}}(t), \qquad (3)$$

where the scaling factor s maximizes the cross-correlation of the monitor and baseline signals.

Figure 1 shows an example of this time-variant calibration applied to one of the stacked traces of monitor 2001 dataset. Because the low- (below about 20 Hz) and high-frequency components of the records appear to be differently affected by noise, differences in acquisition, and effects of seismic processing, these two components are corrected separately. As Figure 1 shows, the calibration procedure reduces the differences between the monitor and baseline traces, and also helps to extract the smoothly-variable time dependences of filter parameters $\Delta t(t)$, $s(t)$, and $t^*(t)$.

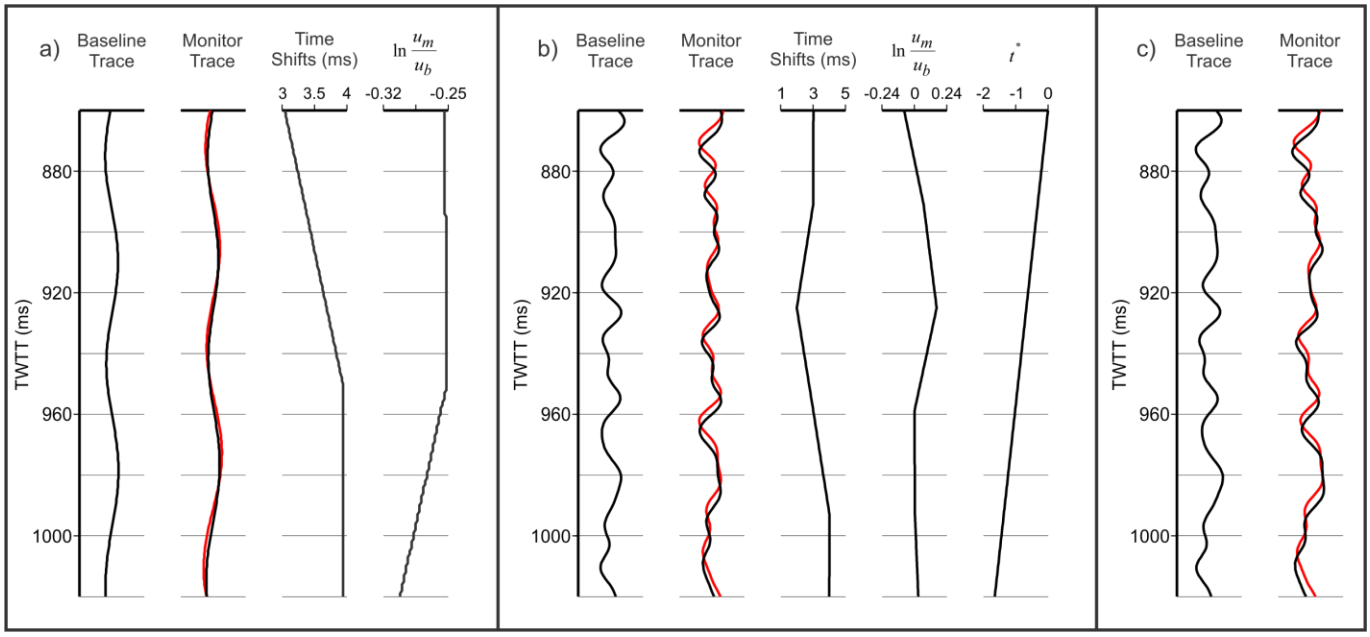

Figure 1: Application of window-based calibration to one record from monitor 2001: a) low-frequency component (below 20 Hz), b) high-frequency component (above 20 Hz), c) complete resulting records. In each panel, black wiggle lines represent the baseline and resulting calibrated monitor records, and red lines show the raw monitor records. Note that the black lines become similar after calibration. Additional graphs in panels a) and b) show the time shifts, logarithms of amplitude scalers $\ln(u_{\text{m}}/u_{\text{b}})$, and spectral slopes t^* (labeled).

Instantaneous-attribute based calibration

Following the time-variant calibration described in the preceding section, we perform an additional calibration step by using instantaneous trace attributes (Taner et al., 1979). The seismic records can be expressed through their attributes a_{r} and θ_{r} as:

$$u_{\text{r}}(t) = a_{\text{r}}(t)\cos\left[\theta_{\text{r}}(t)\right], \qquad (4)$$

where the subscript r = bas or r = mon stands for baseline or monitor records, respectively, a_r denotes the instantaneous amplitude and θ_r is the instantaneous phase. We then measure the time-variant ratio of the instantaneous amplitudes and the difference of instantaneous phases:

$$\alpha(t) = \frac{a_{\text{bas}}(t)}{a_{\text{cmon}}(t)}, \text{ and } \beta(t) = \theta_{\text{bas}}(t) - \theta_{\text{cmon}}(t). \quad (5)$$

These quantities are edited near times t at which either a_{bas} or a_{mon} are low. To achieve such editing, the values of α and β exceeding a pre-set threshold are truncated to zero and filtered by using a smoothing filter. By using the resulting functions $a(t)$ and $\beta(t)$, the calibrated monitor signal is obtained as:

$$u_{\text{cmon}}(t) = \alpha(t) a_{\text{mon}}(t) \cos(\theta_{\text{mon}}(t) + \beta(t)). \quad (6)$$

Time-lapse reflectivity difference

Clearly, for good-quality signals, the above calibration procedure using instantaneous attributes is capable of eliminating the differences between the records practically completely. As we intend to keep the time-lapse signature within the target zone, we utilize this procedure in two passes. In the first pass, we perform calibration by measuring parameters $\Delta t(t)$, $s(t)$, $t^*(t)$, $\alpha(t)$, and $\beta(t)$ outside of the target zone and linearly interpolating them inside the target zone (Figure 1). This pass of calibration should remove the signal differences that are common to the entire records and are not associated with a time-lapse signature of the target zone. In the second pass, we apply the instantaneous-attribute based (high-resolution) calibration to the entire record. This makes the second calibrated monitor record nearly equal the baseline one: $u_{\text{c2mon}}(t) \approx u_{\text{bas}}(t_0)$, and we use the derived calibration parameters to determine the time-lapse change in reflectivity. The time shifts and amplitude variations contained in calibration parameters $\alpha(t)$ and $\beta(t)$ are detailed and accurate, and they allow recovering the differential reflectivity, impedance, and other time-lapse properties of the reservoir.

To derive the differential reflectivity from calibration parameters, let us denote γ_r the amplitude scaling factor measured during the second pass of the calibration procedure:

$$u_{\text{cmon}}(t) = \gamma_r(t_0) u_{\text{c2mon}}(t_0) \approx \gamma_r(t_0) u_{\text{bas}}(t_0), \quad (7)$$

where t_0 and t are the two-way reflection times of the same reflector in the baseline and monitor records. These times are related as:

$$t(t_0) = \int_0^{t_0} \frac{V_0}{V} dt_0, \quad (8)$$

where V_0 is the interval velocity in the baseline record and V is the interval velocity in the monitor. These velocities may be slightly different because of the time-lapse changes within the target reservoir. By differentiating eq. (8) with respect to t_0, the time calibration factor γ_v is obtained as:

$$\frac{1}{\gamma_v} = \frac{V_0}{V} = \frac{dt}{dt_0} = 1 - \frac{d(\delta t)}{dt_0}, \quad (9)$$

where $\delta t = t_0 - t$ is the time shift between the baseline and calibrated monitor records. The time-lapse reflectivity difference accounting for both amplitude variations and the effects of variations in $V(t)$ is:

$$u_{\text{diff}} = u_{\text{c2mon}} \frac{dt}{dt_0} - u_{\text{bas}}. \quad (10)$$

By using eqs. (7) and (9), this difference equals:

$$u_{\text{diff}} = \frac{\gamma_r}{\gamma_v} u_{\text{c2mon}} - u_{\text{bas}} \approx \left(\frac{\gamma_r}{\gamma_v} - 1 \right) u_{\text{bas}}. \quad (11)$$

Thus, the reflectivity difference within the target zone is obtained by scaling the baseline record by a combination of instantaneous-based calibration-parameter functions.

Example

Figure 2 shows segments of one crossline from the stacked time-lapse 3-C 3-D dataset of Weyburn Field. As this Figure shows, an application of the above calibration procedures effectively removes the reflectivity differences outside of the reservoir zone while allowing quantitative measurements of u_{diff} within this zone.

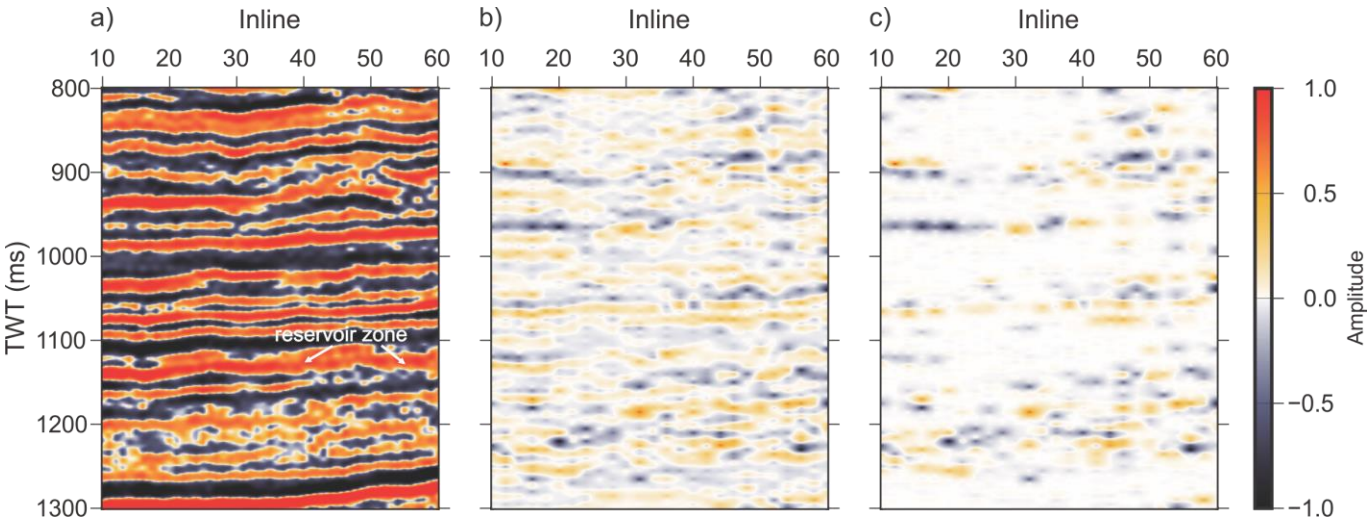

Figure 2: Application to Weyburn CO_2 sequestration study time-lapse dataset: a) Baseline (1999) section with reservoir indicated, b) Reflectivity difference (monitor 2001 minus baseline) after window-based calibration, c) Reflectivity difference after both window-based calibration and instantaneous-based calibration.

Conclusions

The proposed calibration procedures effectively achieve two goals: 1) reducing the differences between time-lapse datasets outside of the target zone, and 2) measuring the time-lapse signatures within the target zone. Because of using instantaneous attributes, the accuracy of the calibration and measurements is improved, which is essential for accurate time-lapse seismic monitoring.

References

Greaves R. J. and Fulp T. J. 1987. Three-dimensional seismic monitoring of an enhanced oil recovery process. Geophysics 52, 1175–1187.

Johnston D. H., McKenny R. S., Verbeek J. and Almond J. 1998. Time-lapse seismic analysis of Fulmar Field. The Leading Edge **17**, 1420–1428.

Lumley D. E. 1995. Seismic time-lapse monitoring of subsurface fluid flow. Ph.D. thesis, Stanford University.

Ross C. P., Cunningham G. B. and Weber D. P. 1996. Inside the crossequalization black box. The Leading Edge **15**, 1233–1240.

Taner M. T., Koehler F. and Sheriff R. E. 1979. Complex seismic trace analysis. Geophysics **44**, 1041-1063.

Wang Y. and Morozov I. B. 2017. Time-lapse acoustic impedance variations after CO_2 injection in Weyburn Field. 87th SEG Annual Meeting, Houston, Expanded Abstracts, 5890–5894.